

**Effect of Sintering Temperature on the Phase Formation,
Microstructure and Electrical Properties of
(Bi_{0.5}Na_{0.5})_{0.93}(Ba_{0.945}Ca_{0.055})_{0.07}(Ti_{0.9896}La_{0.0025}Nb_{0.0025}Sn_{0.0054})O₃ Solid
Solutions Prepared by the Solid State Combustion Technique**

Chittakorn Kornphom^{1*}, Thanakit Inthachim¹. Theerachai Bongkarn^{2, 3}

¹Department of Physics and General Science, Faculty of Science and
Technology, Chiang Mai Rajabhat
University, Chiang Mai, 50300, Thailand;

²Department of Physics, Faculty of Science, Naresuan University,
Phitsanulok, 65000, Thailand

³Research Center for Academic Excellence in Applied Physics, Faculty of
Science, Naresuan University, Phitsanulok, 65000,

*Corresponding author. E-mail: Chittakorn888@gmail.com

ABSTRACT

In this study, the effect of the sintering temperature (950-1150°C for 2 h) on the phase formation, microstructure and electrical properties of (Bi_{0.5}Na_{0.5})_{0.93}(Ba_{0.945}Ca_{0.055})_{0.07}(Ti_{0.9896}La_{0.0025}Nb_{0.0025}Sn_{0.0054})O₃ (BNBC)(TLNS) solid solutions prepared via the solid state combustion technique, using glycine as fuel, were studied. The XRD pattern of all sintered samples exhibited a single perovskite structure with the co-existence of the rhombohedral and tetragonal phases. The average grain size increased with increasing sintering temperature. The density, dielectric constant (at T_r and T_m) and piezoelectric constant (d₃₃) all increased as the sintering temperature increased up to 1100°C and then all values dropped. The sample that showed the highest density (5.87 g/cm³), the highest dielectric constant (ε_r ≅ 1978, ε_m ≅ 6287), and the highest d₃₃ value (228 pC/N), was the sample sintered at 1100°C.

Keywords: (BNBC)(TLNS), solid state combustion technique, phase formation, dielectric, piezoelectric

INTRODUCTION

Recently, lead-free piezoelectric materials with properties that allow them to be used in high performance applications have been the focus of research and development in the electronic industry. Among the many researches developing lead-free piezoelectric ceramics for use in electronic devices, (Bi_{0.5}Na_{0.5})TiO₃ (BNT) based ceramics are considered one of the potential candidate materials to replace toxic lead-based piezoelectric ceramics (Rahman, *et al.* 2014; Jo, *et al.* 2012; Zhang, *et al.* 2008).

Fabrication of Bi_{0.5}Na_{0.5}TiO₃ (BNT)-based solid solutions with a morphotropic phase boundary (MPB) in the perovskite structure, is an effective way to produce ceramics with good piezoelectric coefficient, as reported by many researches (Takenaka, *et al.* 1991; Sasaki, *et al.* 1999; Yoshii, *et al.* 2006; Zhang, *et al.* 2008; Kouna, *et al.* 2008; Hiruma, *et al.* 2008; Lee, *et al.* 2009; Bai, *et al.* 2013; Machado, *et al.* 2017). Takenaka *et al.* (Takenaka, *et al.* 1991) reported relatively

Article history:

Received 18 March 2019;

Accepted 03 May 2019; Available online 24 June 2019

high piezoelectric performance in (1-x)BNT-xBaTiO₃ ((1-x)BNT-xBT) ceramics at the MPB, formed around the composition of x = 0.06-0.07. Machado et al. (Machado, *et al.* 2017) observed a high piezoelectric coefficient (d_{33}) of 180 pC/N in (1-x)BNT-xBT ceramics at an x content of 0.07, with samples poled at 40 kV/cm. Bo Wu et al. (Wu, *et al.* 2012) reported that introducing 6 mol% of (Ba_{0.98}Ca_{0.02})(Ti_{0.94}Sn_{0.06})O₃ in BNT produced ceramics with a MPB and a high piezoelectric constant ($d_{33} \approx 170$ pC/N). Then, Chittakorn et al (Kornphom, *et al.* 2018) reported a high piezoelectric coefficient, d_{33} , of 189 pC/N in 0.94(Bi_{0.5}Na_{0.5}TiO₃)-0.06(Ba_{0.945}Ca_{0.055})(Ti_{0.91}Sn_{0.09})O₃ (0.94BNT-0.06BCTS) ceramics, fabricated by the solid state combustion technique, sintered at 1150°C for 2 h. After that, Rui-Fang Ge et al (Ge, *et al.* 2017) studied the influence of La³⁺ and Nb⁵⁺ on 0.85Bi_{0.5}Na_{0.5}TiO₃-0.11Bi_{0.5}K_{0.5}TiO₃-0.04BaTiO₃ (BNT-BKT-BT) ceramics, which showed a phase transformation from a mix of rhombohedral and tetragonal to a pseudocubic symmetry with high field-induced strain. With increasing La³⁺ and Nb⁵⁺ content, the normal ferroelectric-to-ergodic relaxor (FE-to-ER) transition temperature (T_{F-ER}) reduced from 120°C to below room temperature (RT). The largest electro-strain of 0.46% was obtained from the samples with La³⁺ and Nb⁵⁺ content at 0.0050 and under an applied electric field of 7.5 kV/mm. Hence, the interest in doping BNT-BCTS ceramics with La³⁺ and Nb⁵⁺ at compositions that induce a MPB.

From a review of the literature, it can be seen that adding La³⁺ and Nb⁵⁺ to 0.93(Bi_{0.5}Na_{0.5}TiO₃)-0.07(Ba_{0.945}Ca_{0.055})(Ti_{0.91}Sn_{0.09})O₃ (0.93BNT-0.07BCTS) ceramics, prepared by the solid state combustion technique has not been studied. In this research, we report on the the fabrication of 0.93BNT-0.07BCTS solid solutions doped with La³⁺ and Nb⁵⁺ at x=0.005 according to the formula (Bi_{0.5}Na_{0.5})_{0.93}(Ba_{0.945}Ca_{0.055})_{0.07}(Ti_{0.9896}La_{0.0025}Nb_{0.0025}Sn_{0.0054})O₃ (BNBC)(TLNS) via the solid state combustion technique. The influence of the sintering temperature on the phase formation, morphology, and electrical properties in this ceramics were investigated.

EXPRIMENT DETAIL

(Bi_{0.5}Na_{0.5})_{0.93}(Ba_{0.945}Ca_{0.055})_{0.07} (Ti_{0.9896}La_{0.0025}Nb_{0.0025}Sn_{0.0054})O₃ (BNBC)-(TLNS) ceramics were synthesized by the solid state combustion technique using glycine (C₂H₅NO₂) as fuel. The raw materials were obtained from the high purity reagent grade sources of Bi(NO₃)₃.5H₂O (99%), Na(NO₃)₂ (99%), TiO₂ (99%), Ba(NO₃)₂ (99%), CaCO₃ (99.0%), SnO₂ (99.0%), La₂O₃ (99%), Nb₂O₅ (99%), and C₂H₅NO₂ (95.0%). The raw materials were weighed following the given composition and were mixed by ball milling in ethanol for 24 h. Afterwards, the suspensions were dried and sieved into a fine powder. After drying, the powders were mixed with glycine in a ratio of 1:2 and then the mixed powders were calcined at 650°C for 2 h in air (Kornphom, *et al.* 2018). Thereafter, polyvinyl alcohol (PVA: 5 wt.% aqueous solution) was added into the calcined powders and ball-milled again for 24 h. Next, the mixed calcined powders were pressed into disks under a pressure of 1000 kg/cm²

in a mold which has a diameter of 15 mm. Finally, all green bodies were sintered at temperatures between 950 - 1150°C for 2 h in air with a heating rate of 5°C/min and allowed to cool down naturally.

The phase transition of the sintered samples were analyzed by X-ray diffraction (XRD). While the morphology was analyzed by scanning electron microscopy (SEM). The average grain size of the sintered samples was determined by using the linear interception method on SEM images of polished samples which had been thermally etched for 10 min at a temperature 100-110°C below the sintering temperature. The density of the sintered samples was measured using the Archimedes method with distilled water as the medium. The dielectric properties were measured by a LCR meter (Agilent 4263B) with a frequency of 1-100 kHz. To measure the piezoelectric properties, the sintered samples were polished to 1 mm thickness and silver paste (Heraeus, D11402) was painted on both sides to form electrodes and then annealed at a temperature of 500°C for 30 min. Poling sintered samples were carried out at 40°C in a silicon oil bath by an applied field of 5 kV/cm for 20 min (Kornphom, *et al.* 2018). All poling samples were allowed to set for 24 h prior to measuring the piezoelectric properties. The piezoelectric properties was measured by a Berlincourt d_{33} meter (Sinocera, YE2730A).

RESULTS AND DISCUSSION

The phase formation of (BNBC)(TLNS) ceramics as a function of the sintering temperature was investigated by XRD and all XRD patterns are presented in Fig 1 (a)-(c). The XRD results showed that all sintered samples formed a pure perovskite structure, as the 2θ between 10 to 60° in the XRD patterns in all matched with the JCPDS files no.36-0340 and 03-0725. The XRD patterns also had no impurity phase (Fig.1 (a)) which indicated that La^{3+} and Nb^{5+} easily substituted into B-sites of the (BNBC)(TLNS) lattice structure forming a complete solid solution.

A more thorough investigation of the effect of the sintering temperature on the structural features, including the phase characteristics, of the samples could be obtained by analyzing the amplified 2θ XRD patterns at ~40° and 47°, which are shown in Fig. 1(b) and (c). A rhombohedral (R) perovskite phase can be identified by dual (003)/(021)_R peaks at a lower angle (~40°) and a single (202)_R peak at a higher angle (~47°) (Bhupaijit, *et al.* 2015; Herabut, *et al.* 1997; Gou, *et al.* 2012). And a tetragonal (T) phase can be identified by a single peak of (111)_T at a lower angle and dual split peaks of (002)/(200)_T at a higher angle (Bhupaijit, *et al.* 2015; Gou, *et al.* 2012). In this work, at a sintered temperature of 950°C, the XRD pattern exhibited twisted peaks around 40° and a broad double peaks around 47° (Fig.1 (b) I) and (Fig.2 (c) I) which indicates that an incomplete sintering process resulted in an unstable crystalline structure. As the sintering temperature increased from 1000 to 1050°C, the peak around 40° showed broad double peaks of (003)/(021)_R (Fig. 1 (b) II, III) and split double peaks of (002)/(200)_T at peak position of 47° were observed (Fig. 1 (c) II, III), which indicated that these samples showed the coexistence of the rhombohedral and tetragonal phases (R+T). For the sample sintered at 1100°C, the peak position at

around 40° showed a more symmetry peak of $(111)_T$ (Fig. 1 (b) IV) and split double peaks of $(002)/(200)_T$ at 47° (Fig. 1(c) IV), which indicates that this sample was dominated by the tetragonal phase. Moreover, it was observed that the peaks around 40 and 47° moved to a slightly lower angle when the sintering temperature increased from 950 to 1100°C (Figure 1 (b) I-IV and (c) I-IV), indicating that the unit cell value slightly enlarged. When the sintering temperature was increased to 1150°C , the peaks around 40° and 47° showed a broader $(111)_T$ peak and $(002)/(200)_T$ peaks, while, both peak positions shifted to higher angles, indicating the unit cell value slightly shrank (Fig.2 (b) V and (c) V). The variation in the phase formation and the unit cell volume in the samples sintered at high temperatures may be due to the distortion of the crystal structure and the reduction of the crystallinity due to the evaporation of Bi_2O_3 and / or Na_2O (Kornphom, *et al.* 2018).

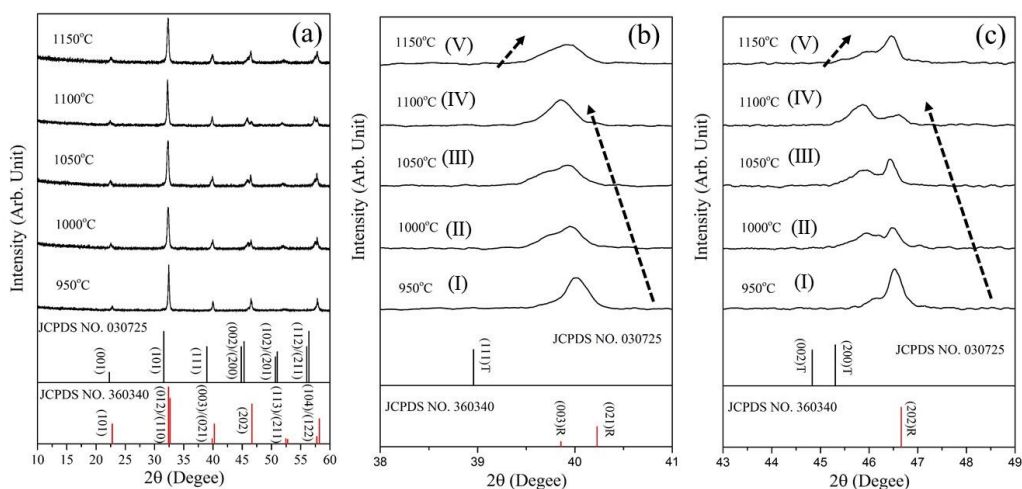


Fig. 1 XRD patterns of the (BNBC)(TLNS) solid solution as a function of sintering temperature (a) $2\theta = 10-60^\circ$, (b) $2\theta = 38-41^\circ$ and (c) $2\theta = 43-49^\circ$.

SEM images of the surface morphology of the sintered (BNBC)(TLNS) solid solutions, after being polished and thermally etched, are shown in Fig. 2 (a)-(e). The grains of all sintered samples showed a polygonal shape. It was found that large porous structures and small grains were observed on the surface of the sample at the low sintering temperature of 950°C (Fig. 2 (a)). Then, the porous structure reduced and the grains continuously grew when the sintering temperature increased from 1000°C to 1100°C (Fig. 2 (b)-(d)). For the sample sintered at a temperature of 1150°C , the grains abnormally grew and the grain boundary began to melt (Fig. 3 (e)) which may be due to the fact that Bi_2O_3 or Na_2O , with low-boiling points, could have evaporated at higher sintering temperatures (Kornphom, *et al.* 2018). The average grain size of all sintered ceramics increased with increasing sintering temperature as seen in Table 1.

The density of the (BNBC)(TLNS) solid solutions with various sintering temperatures were obtained using the Archimedes technique. The apparent density increased from 5.35 g.cm^{-3} to 5.87 g.cm^{-3} by increasing the sintering temperature from 950 to 1100°C , a higher sintering temperature reduced the sample density (Table. 1). The sample sintered at a temperature of 1100°C showed the highest density (5.87 g.cm^{-3}). The density results of all sintered samples corresponded well with the microstructure results.

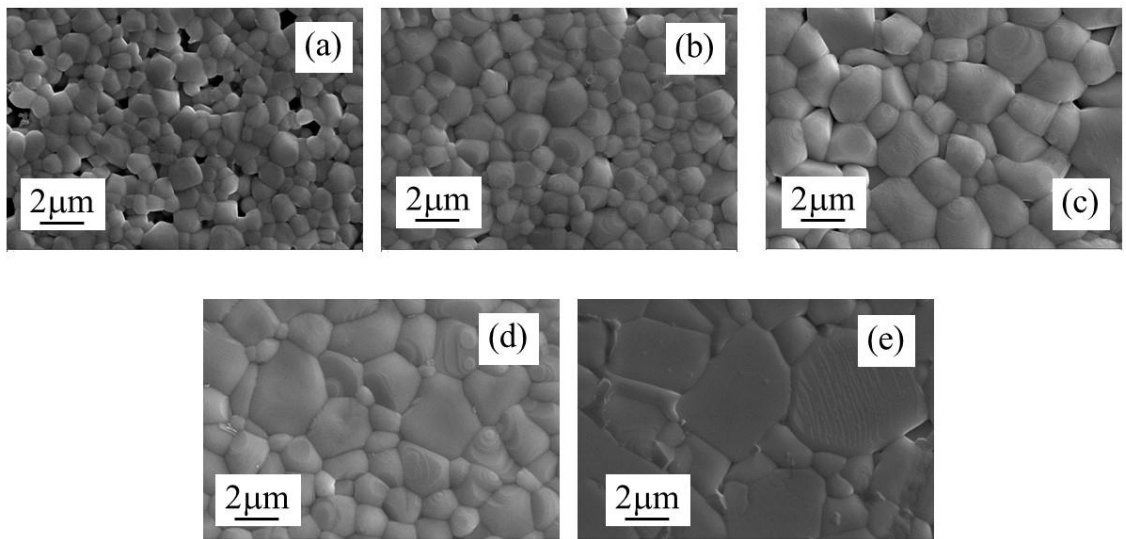


Fig. 2. The SEM image of the (BNBC)(TLNS) solid solution sintered at (a) 950°C , (b) 1000°C , (c) 1050°C , (d) 1100°C and (e) 1150°C for 2 h.

The temperature dependent dielectric responses of the unpoled and poled (BNBC)(TLNS) solid solutions sintered at 1100°C for 2 h (i.e. the highest density samples) measured at the frequencies of 1 kHz, 10 kHz and 100 kHz are presented in Fig. 3(a)-(b). It was found that the unpoled sample exhibited broad dielectric anomalies as shown in Fig. 3 (a). For the poled sample, the dielectric anomalies exhibited differentiation of two dielectric curves as observed in Fig. 3 (b). The first dielectric curve was clearly observed from the dielectric constant and dielectric loss at a temperature around 50°C with a marginal frequency dispersion (Fig. 3 (b)). This dielectric behavior around 50°C refers to the phase transition temperature of normal ferroelectric to relaxor ferroelectric (T_{FR}) and can be attributed to coexisting polar nanoregions (PNRs) of different symmetries (Kornphom, *et al.* 2016; Jo, *et al.* 2011; Rahman, *et al.* 2015). The second curve was found at higher temperatures around 250°C which is called the temperature of the maximum dielectric constant (T_{m}) and is caused by the thermal evolution of ferroelectric PNRs of R3c and weakly polar P4bm symmetry (Fig. 3 (b)) (Jo, *et al.* 2011; Rahman, *et al.* 2015).

The temperature dependence of the dielectric response of the unpoled and poled (BNBC)(TLNS) solid solutions sintered at different temperatures measured at 1 kHz are showed in Fig. 4 (a) and (b). For unpoled samples, the dielectric anomalies exhibited broad curves in all sintered samples. It can be seen that the T_m values of all sintered samples were between 250 and 287°C as listed in Table 1. The sample sintered at 950°C couldn't be poled because it broke down under the high electric field. For the dielectric anomalies of the poled samples, it can be observed that the samples sintered at 1000-1150°C showed two dielectric curves of T_{F-R} and T_m at temperatures around 50°C and 280°C (T_m), respectively, Fig. 4 (b). For T_{FR} values of the samples sintered between 1000-1150°C, it was found that T_{FR} slightly increased from 52 to 56°C when the sintering temperature increased from 1000°C to 1150°C (Table 1). The change of T_m (the unpoled samples) and T_{F-R} values (the poled samples) in the (BNBC)(TLNS) solid solution at difference sintering temperature may be caused from the phase distortion and compositional discrepancy arising due to the volatility of Bi_2O_3 or Na_2O at higher temperatures (Kornphom, *et al.* 2018), and corresponded well with the findings of the phase formation, microstructure and density.

The dielectric constant (ϵ) at room temperature (T_r) and dielectric constant at T_m of the unpoled (BNBC)(TLNS) solid solution increased from 1485 to 1978 and 4500 to 6287, respectively, when the sintered temperature increased from 950-1100°C and then dropped in values as listed in Table 1. The dielectric loss at T_m ($\tan \delta_m$) for all samples are listed in Table 1. Good dielectric responses were attained by the highly dense ceramics with well-developed crystalline structures, which corresponded to the phase formation, morphology and density results.

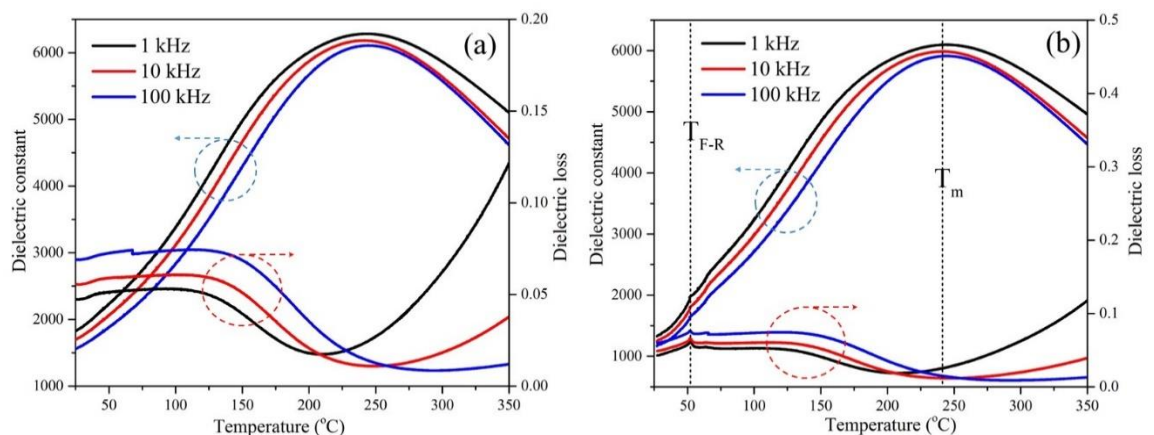


Fig. 3 Temperature dependence of the dielectric constant and loss of the (BNBC)(TLNS) solid solutions sintered at 1100°C for 2 h for the (a) unpoled sample and (b) poled sample.

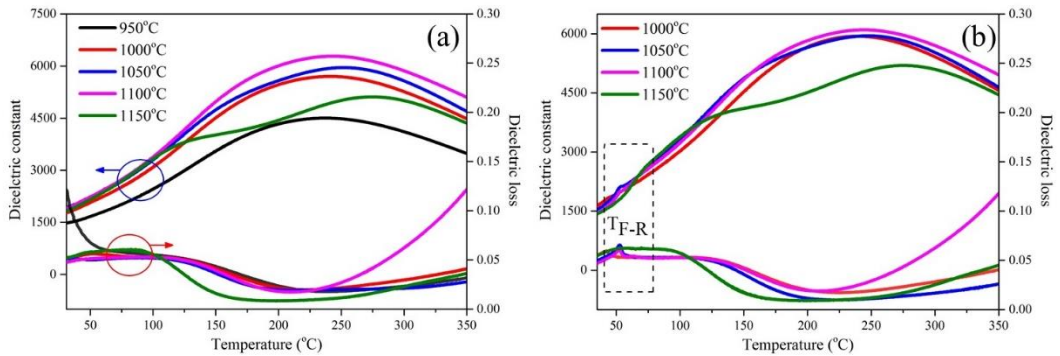


Fig. 4 Temperature dependence of the dielectric constant and loss of the (BNBC)(TLNS) solid solutions sintered at various temperatures for the (a) unpoled sample and (b) poled sample.

The measured piezoelectric coefficient (d_{33}) of the (BNBC)(TLNS) solid solutions with sintering temperature between 1000°C and 1150°C is listed in Table 1. It can clearly be observed that the d_{33} value increased from 158 pC/N to 228 pC/N when the sintering temperature increased from 1000°C to 1100°C . At the sintering temperature of 1150°C , the d_{33} value decreased. The highest d_{33} value of 228 pC/N was reached from the sample sintered at 1100°C . The improved dielectric and piezoelectric properties in the (BNBC)(TLNS) solid solution as a function of sintering temperature can be explained from the phase transition zone with the R+T coexisting phases, the well-developed morphology and good density, enhancing domain reorientation and domain wall motion, resulting in the polarization to be easily switchable (Kornphom, *et al.* 2018). These factors reduce the volume fraction of the grain boundaries and inhibit the trapping of space charges at the grain boundaries (Herabut, *et al.* 1997; Kornphom, *et al.* 2016; Jo, *et al.* 2011). When the sintering temperature increased up to 1150°C , the dielectric constant, and d_{33} value reduced because of the volatilization of Bi_2O_3 or Na_2O at higher sintering temperatures which degenerated the electrical properties.

Table 1 Average grain size, density, dielectric and piezoelectric properties of (BNBC)(TLNS) solid solution at different sintering temperatures

Sintering temperature (°C)	Average grain size (μm)	Density (g/cm^3)	$T_{\text{F-R}}$ (°C)	T_{m} (°C)	ϵ_{r}	$\tan \delta$ at T_{r}	ϵ_{m}	$\tan \delta$ at T_{m}	d_{33} (pC/N)
950	1.14±0.18	5.35	-	233	1485	0.130	4500	0.030	-
1000	1.55±0.25	5.64	42	237	1692	0.053	5712	0.028	158
1050	1.96±0.51	5.78	52	247	1876	0.051	5924	0.024	189
1100	2.50±0.77	5.87	52	242	1978	0.047	6287	0.021	228
1150	2.89±0.80	5.59	56	275	1835	0.052	5122	0.016	169

CONCLUSIONS

In this study, high performance (BNBC)(TLNS) solid solutions were synthesized by the solid state combustion technique. The effect of the sintering temperature on the phase formation, microstructure, density and electrical properties were investigated. The (BNBC)(TLNS) solid solutions exhibited a pure perovskite phase with co-existing rhombohedral and tetragonal phases in all sintered samples. The good microstructure, the best density, and excellent electrical properties ($\epsilon_{\text{r}} \cong 1978$, $\epsilon_{\text{m}} \cong 6287$, and d_{33} of 228 pC/N) were obtained from the samples sintered at a temperature of 1100°C for 2 h. From these results, a high piezoelectric coefficient in (BNBC)(TLNS) solid solutions, using an optimal sintering temperature, is a promising candidate for lead-free ferroelectric ceramics and can replace Pb-based ceramics for application in electronic devices.

ACKNOWLEDGEMENTS

The authors wish to thank the Department of Physics, Faculty of Science, Naresuan University and the Department of Physics and General Science, Faculty of Science and Technology, Chiang Mai Rajabhat University for their supporting facilities. Thanks are also given to Dr. Kyle V. Lopin for his help in editing the manuscript.

FUNDING

This work was financially supported by the research fund of Chiang Mai Rajabhat University.

REFERENCES

- Rahman, JU., Hussain, A., Maqbool, A., Song, TK., Kim, WJ., Kim, SS. *et al.* (2014). Dielectric, ferroelectric and field-induced strain response of lead-free BaZrO₃-modified Bi_{0.5}Na_{0.5}TiO₃ ceramics. *Current Applied Physics*, 14, 331–336.
- Jo, W., Dittmer, R., Acosta, M., Zang, J., Groh, C., Sapper, E., Wang, K. and Rödel, J. (2012). Giant electric-field-induced strains in lead-free ceramics for actuator applications—status and perspective. *Journal of Electroceramics*, 29, 71–93.
- Zhang, YR., Li, JF., Zhang, BP. and Peng, CE., (2008). Piezoelectric and ferroelectric properties of Bi-compensated (Bi_{1/2}Na_{1/2})TiO₃–(Bi_{1/2}K_{1/2})TiO₃ lead-free piezoelectric ceramics. *Journal of Applied Physics*, 103, 074109.
- Takenaka, T., Maruyama, K. and Sakata, K. (1991). Electrical properties and depolarization temperature of (Bi_{1/2}Na_{1/2})TiO₃–BaTiO₃ system for lead-free piezoelectric ceramics, *Japanese Journal of Applied Physics*, 30, 2236–2239.
- Sasaki, A., Chiba, T., Mamiya, Y. and Otsuki, E. (1999) Dielectric and piezoelectric properties of (Bi_{0.5}Na_{0.5})TiO₃–(Bi_{0.5}K_{0.5})TiO₃ systems, *Japanese Journal of Applied Physics*, 38, 5564–5567.
- Yoshii, K., Hiruma, Y., Nagata, H. and Takenaka T., (2006). Electrical properties and depolarization temperature of (Bi_{1/2}Na_{1/2})TiO₃–(Bi_{1/2}K_{1/2})TiO₃ lead-free piezoelectric ceramics, *Japanese Journal of Applied Physics*, 45, 4493–4496.
- Zhang, S.T., Kouna, A.B., Emil, A. and Deng, Y. (2008). Temperature-dependent electrical properties of 0.94Bi_{0.5}Na_{0.5}TiO₃–0.06BaTiO₃ ceramics, *Journal of the American Ceramic Society*. 91, 3950–3954.
- Kouna, A.B., Zhang, S.T., Jo, W., Granzow, T. and Rodel, J. (2008). Morphotropic phase boundary in (1-x)Bi_{0.5}Na_{0.5}TiO₃–xK_{0.5}Na_{0.5}NbO₃ lead-free piezoceramics, *Applied Physics Letter*, 92, 222902.
- Hiruma, Y., Imai, Y., Watanabe, Y., Nagata, H. and Takenaka, T. (2008). Large electro strain near the phase transition temperature of (Bi_{0.5}Na_{0.5})TiO₃–SrTiO₃ ferroelectric ceramics, *Applied Physics Letter*, 92, 262904.
- Lee, WC., Lee, YF., Tseng, MH., Huang, CY. and Wu, YC (2009) Crystal structure and ferroelectric properties of (Bi_{0.5}Na_{0.5})TiO₃–Ba(Zr_{0.05}Ti_{0.95})O₃ piezoelectric ceramics, *Journal of the American Ceramic Society*. 92, 1069–1073.

- Bai, W., Bian, Y., Hao, J., Shen, B., Zhai, J. and Zhang, S. (2013). The composition and temperature- dependent structure evolution and large strain response in $(1-x)(\text{Bi}_{0.5}\text{Na}_{0.5})\text{TiO}_3-x\text{Ba}(\text{Al}_{0.5}\text{Ta}_{0.5})\text{O}_3$ ceramics, *Journal of the American Ceramic Society*, 96, 246–252.
- Machado, R., dos Santos, V.B., Ochoa, D. A., Cerdeiras, E., Mestres, L. and Garcia, J. E. (2017). Elastic, dielectric and electromechanical properties of $(\text{Bi}_{0.5}\text{Na}_{0.5})\text{TiO}_3\text{-BaTiO}_3$ piezoceramics at the morphotropic phase boundary region. *Journal of alloys and compounds*. 690, 568-574.
- Wu, B., Xiao, D., Wu, W., Zhu, J., Chen, Q., Wu, J. (2012). Microstructure and electrical properties of $(\text{Ba}_{0.98}\text{Ca}_{0.02})(\text{Ti}_{0.94}\text{Sn}_{0.06})\text{O}_3$ -modified $\text{Bi}_{0.51}\text{Na}_{0.50}\text{TiO}_3$ lead-free ceramics, *Ceramics International*, 38, 5677-5681.
- Kornphom, C., Rittisak, J., Laowanidwatana, A. and Bongkarn, T. (2018). Enhanced dielectric and ferroelectric behavior in 0.94BNT-0.06BCTS lead free piezoelectric ceramics synthesized by the solid state combustion technique. *Integrated Ferroelectrics*, 187, 20-32.
- Ge, RF., Zhao, Z., Duan, S., Kang, X., Lv, Y., Yin, D. and Dai, YJ. (2017). Large electro-strain response of La^{3+} and Nb^{5+} co-doped ternary $0.85\text{Bi}_{0.5}\text{Na}_{0.5}\text{TiO}_3\text{-}0.11\text{Bi}_{0.5}\text{K}_{0.5}\text{TiO}_3\text{-}0.04\text{BaTiO}_3$ lead-free piezoelectric ceramics. *Alloys and Compounds*, 724, 1000-1006.
- Bhupaijit, P., Kornphom, C., Vittayakorn, N. and Bongkarn, T. (2015). Structural, microstructure and electrical properties of La_2O_3 - doped $(\text{Bi}_{0.5}\text{Na}_{0.68}\text{K}_{0.22}\text{Li}_{0.05})\text{TiO}_3$ lead-free piezoelectric ceramics synthesized by the combustion technique. *Ceramics International*, 41, 81-86.
- Herabut, A. and Safari, AM. (1997). Processing and electromechanical properties of $(\text{Bi}_{0.5}\text{Na}_{0.5})_{1-1.5x}\text{La}_x\text{TiO}_3$ ceramics. *Journal of the American Ceramic Society*, 80, 2954-2958.
- Gou, Q., Wu, JG., Li, AG., Wu, B., Xiao, DG. and Zhu, JG. (2012). Enhanced d_{33} value of $\text{Bi}_{0.5}\text{Na}_{0.5}\text{TiO}_3\text{-(Ba}_{0.85}\text{Ca}_{0.15})(\text{Ti}_{0.90}\text{Zr}_{0.10})\text{O}_3$ lead-free ceramics. *Alloys and Compounds*, 521, 4 –7.